SCIENTIFIC PAPER
Published: June 12, 2025
https://doi.org/10.13167/2025.30.15

A simple triangular finite element model for analysing the linear static behaviour of thick sandwich plates with equivalent material properties

Hichem Belaid[1], Hassina Ziou[2] and Mohammed Himeur[1]

[1] *Department of Civil Engineering and Hydraulic, Laboratory of Civil and Hydraulic Engineering, University May 8, 1945, Guelma, Algeria*

[2] *National Centre of Integrated Studies and Research on Building Engineering (CNERIB), Souidania, Algiers, Algeria*

Corresponding author:
Hassina Ziou
h.ziou@cnerib.edu.dz

Received:
November 20, 2024

Revised:
April 7, 2025

Accepted:
April 8, 2025

Published:
June 12, 2025

Citation:
Belaid, H.; Ziou, H.; Himeur, M. A simple triangular finite element model for analysing the linear static behaviour of thick sandwich plates with equivalent material properties. *Advances in Civil and Architectural Engineering,* 2025, 16 (30), pp. 262-286. https://doi.org/10.13167/2025.30.15

ADVANCES IN CIVIL AND ARCHITECTURAL ENGINEERING (ISSN 2975-3848)

Faculty of Civil Engineering and Architecture Osijek
Josip Juraj Strossmayer University of Osijek
Vladimira Preloga 3
31000 Osijek
CROATIA

Abstract:
This study presents a simple triangular finite element model for analysing the linear static behaviour of thick sandwich plates. What sets this work apart is its unique combination of the deformation approach with Airy's function and analytic integration. The triangular plate finite element (TPFE) model using the Airy function consists of three nodes, each with three degrees of freedom: one transverse displacement and two rotations. Interpolation functions for strain, displacements, and stresses are derived using equilibrium conditions. The selection of bi-harmonic polynomial functions is based on the evolution of the Airy solutions. The basic stiffness matrix is evaluated using the variational principle and analytical integration approach. Additionally, the equivalent material properties for a sandwich plate are obtained using a simple mathematical formula. The numerical results are evaluated and validated using analytical and numerical solutions. The comparison demonstrates the efficiency and accuracy of the TPFE element. Furthermore, the study presents the effects of geometrical parameters, such as thickness configurations and length-to-thickness ratios, as well as end-boundary and load conditions, on the deflection behaviour of the sandwich plates.

Keywords:
triangular finite element; analytical integration; deformation approach; Reissner–Mindlin theory; Airy function; sandwich plate; equivalent material properties

1 Introduction

Composite materials offer several advantages over traditional materials. They provide numerous functional benefits in terms of weight, mechanical and chemical resistance, maintenance, and design flexibility. They contribute to extending the lifespan of certain equipment owing to their unique properties. In addition, they expand design possibilities by enabling lighter structures and complex, multifunctional forms, leading to innovations in construction, automotive, and industrial equipment. Composite materials provide industrial professionals and designers with new opportunities to combine functions, shapes, and materials in their creations. It is an increasingly efficient system, with weight and multifunctionality being key principles in the development of new design and industrialisation processes, expanding technical possibilities, and more effectively addressing otherwise conflicting needs, such as weight and functionality, which conventional homogeneous materials struggle to meet.

Next, a brief review of relevant literature is presented: Linke et al. [1] conducted static and stability analyses of a sandwich plate using the finite element method (FEM), considering a three-layered sandwich model and based on the classical Kirchhoff–Love hypothesis for the face sheets.

References [2-5] investigated the challenges associated with the static and dynamic deformations of composite materials. focused on three-layer plates [2-4]. They also investigated the response of these plates to various loads and examined the vibrations of circular composite plates on elastic foundations [5]. Pham et al. [6] developed an innovative first-order mixed-plate element for the static-bending and free-vibration analysis of functionally-graded sandwich plates. Hadji and Tounsi [7] introduced an advanced shear deformation theory to investigate the stress distribution and static deflection of a sandwich plate composed of a simply supported porous functionally graded material (FGM). They also extensively examined the impact of various influencing factors on the bending performance. Demirhan and Taskin [8] investigated the bending behaviour of symmetric and asymmetric sandwich plates made of an FGM under a uniformly distributed load applied to the top surface. Hirane et al. [9] proposed a four-sided eight-node C0 element to analyse the static and free-vibration behaviours of functionally graded sandwich panels. The proposed delamination model included a high-order displacement field of the core and a first-order displacement field of the cover layer, ensuring the continuity of the displacement at the layer interface.

Sahoo and Singh [10] introduced the hyperbolic zigzag theory to analyse the static responses of multi-layered and sandwich composite panels using an FEM model. Moradi-Dastjerdi and Aghadavoudi [11] examined the static behaviour of sandwich plates by employing molecular dynamics simulations and used the Halpin–Tsai equation to assess the material properties of defective CNT/polymer outer layers. Sahoo and Singh [12] also introduced the trigonometric zigzag theory incorporating a specific secant function to analyse the static structural behaviour of laminated composites and sandwich plates. This theory considered shear-strain shape functions and assumed a non-linear distribution of in-plane displacement across the thickness. Nawariya et al. [13] used the ANSYS APDL FEM to analyse the static and harmonic behaviours of a sandwich plate made of orthotropic and isotropic composites. They applied the Reissner-Mindlin theory and observed the effect of increasing the ratio of the thickness of a face sheet to the plate depth on the static, vibration, and harmonic responses.

The proposed theoretical model, which incorporated only four governing equations without a shear correction factor, satisfied the zero-traction boundary conditions on the plate surfaces. Numerous investigations on modelling the dynamic response of intact composite/sandwich structures have been conducted [14-17].

Recent studies have investigated the mechanical behaviour, free vibration, buckling, and bending–torsional responses of functionally graded and composite thin-walled beams using advanced and refined beam theories, including 1D and 3D and Saint-Venant-based approaches [18-24].

Although some previous studies have addressed the analysis of FGM beams, nanobeams, and perforated nanobeams, including investigations on their modal behaviour, bending response, and buckling characteristics [25-28].
This study introduces a straightforward triangular finite element model to examine the linear static behaviour of thick sandwich plates. The model named “TPFE” using the Airy function is unique in that it applies a deformation approach involving the Airy function and analytic integration. The TPFE consists of three nodes, each with three degrees of freedom (DOF): one transverse displacement (w_i) and two rotations (θ_{xi} and θ_{yi}). This accurately represents the rigid-body displacement modes. The strain, displacement, and stress-interpolation functions were derived based on equilibrium conditions. The choice of polynomial bi-harmonic functions is influenced by the progression of the Airy function solutions. The fundamental stiffness matrix was calculated using the variational principle and analytical integration approach. In addition, the equivalent material properties of sandwich plates are determined using a simple mathematical formula. A combination of tabular and graphical results is presented to highlight the effects of various parameters, such as geometrical factors (thickness configurations and length-to-thickness ratios), as well as end-boundary and load conditions, on the static behaviour of the sandwich plates.
The results presented in this paper will serve as a valuable reference for future research on the static behaviour of sandwich plates.

2 Finite element formulation

2.1 Triangular finite element model

2.1.1 Characteristics

A finite element model of a thick triangular plate with planar elasticity is proposed (Figure 1). Each node in this model had three DOF: one displacement w_i and two rotations θ_{xi} and θ_{yi}. This model was formulated using the deformation model, which means that interpolation polynomials were primarily established to describe the deformation fields.

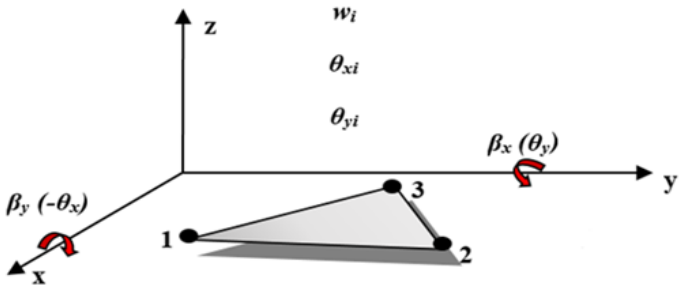

Figure 1. Triangular element with three degrees of freedom per node

Subsequently, the interpolation functions of the displacement fields were obtained by integrating these polynomials. For zero body forces, the approximation functions are selected by introducing the Airy function ϕ (x, y), which allows the equilibrium conditions problem to be reduced:

$$\begin{bmatrix} \frac{\partial}{\partial x} & 0 & \frac{\partial}{\partial y} \\ 0 & \frac{\partial}{\partial y} & \frac{\partial}{\partial x} \end{bmatrix} \begin{Bmatrix} \sigma_x \\ \sigma_x \\ \tau_{xy} \end{Bmatrix} = \begin{Bmatrix} 0 \\ 0 \end{Bmatrix} \quad (1)$$

This leads to the bi-harmonic equation:

$$\nabla^4\phi(x,y) = 0 \tag{2}$$

where:

$$\sigma_x = \frac{\partial^2\phi(x,y)}{\partial y^2} \quad \sigma_y = \frac{\partial^2\phi(x,y)}{\partial x^2} \quad \tau_{xy} = \frac{\partial^2\phi(x,y)}{\partial x \partial y} \tag{3}$$

For isotropic materials with a plane state of stress, the deformation is related to the stress via the following relationship (Hooke's law):

$$\begin{Bmatrix}\sigma_x\\ \sigma_y\\ \tau_{xy}\end{Bmatrix} = \frac{E}{1-\nu^2}\begin{bmatrix}1 & \nu & 0\\ \nu & 1 & 0\\ 0 & 0 & \frac{1-\nu}{2}\end{bmatrix}\begin{Bmatrix}\varepsilon_x\\ \varepsilon_y\\ \gamma_{xy}\end{Bmatrix} \text{ or again } \begin{Bmatrix}\varepsilon_x\\ \varepsilon_y\\ \gamma_{xy}\end{Bmatrix} = \frac{1}{E}\begin{bmatrix}1 & -\nu & 0\\ -\nu & 1 & 0\\ 0 & 0 & 2(1+\nu)\end{bmatrix}\begin{Bmatrix}\sigma_x\\ \sigma_y\\ \tau_{xy}\end{Bmatrix} \tag{4}$$

By introducing the Airy function ϕ (*x*, *y*), the deformations can be represented as follows:

$$\begin{cases}\varepsilon_x = \frac{1}{E}\left(\frac{\partial^2\phi(x,y)}{\partial y^2} - \nu\frac{\partial^2\phi(x,y)}{\partial x^2}\right)\\ \varepsilon_y = \frac{1}{E}\left(\frac{\partial^2\phi(x,y)}{\partial x^2} - \nu\frac{\partial^2\phi(x,y)}{\partial y^2}\right)\\ \gamma_{xy} = \frac{-2(1+\nu)}{E}\left(\frac{\partial^2\phi(x,y)}{\partial x \partial y}\right)\end{cases} \tag{5}$$

The bi-harmonic solutions of the Airy function ϕ (*x*, *y*) used to construct the interpolation polynomials for the strain field are given in [29]. Each node of the considered element had three DOF, which resulted in nine relevant constants in the displacement field formulated using the strain method.
Therefore, the first nine solutions were considered (refer to Appendix A):

- Three terms for rigid-body motion.
- Three terms for linear displacement.
- Three terms for higher-order displacement.

2.2 Reissner–Mindlin plate theory

This theory is essentially based on the Reissner-Mindlin assumption that the normal lines to the undeformed mid-plane remain straight but not necessarily perpendicular to the mean surface after deformation, thus facilitating transverse shear deformation effects (Figure 2).

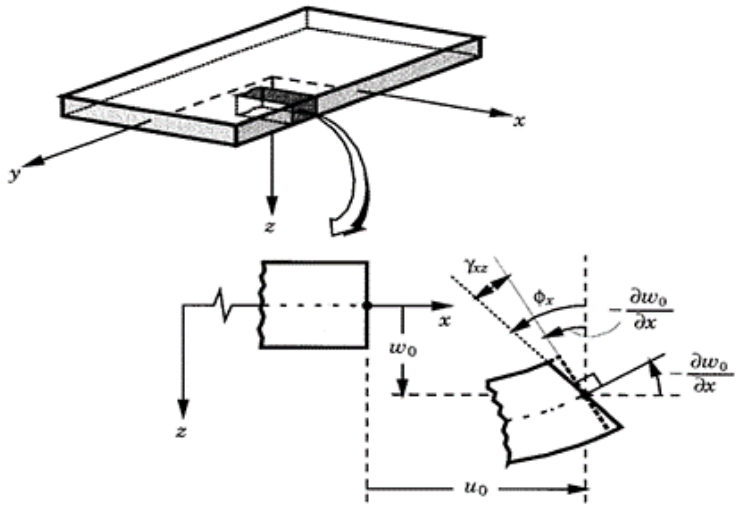

Figure 2. Deformed and undeformed geometries of an edge of a plate under the Reissner-Mindlin assumption

2.2.1 Displacement field

Based on the Reissner-Mindlin plate theory, the displacement field at any point in the plate section can be expressed as:

$$\begin{cases} u(x,y,z) = z\beta_x(x,y) = z\phi_y(x,y) \\ v(x,y,z) = z\beta_y(x,y) = -z\phi_x(x,y) \\ w(x,y,z) = w(x,y) \end{cases} \quad (6\text{-a})$$

where *u* and *v* are the components of the in-plane displacements that vary linearly along the z-axis, whereas w is the constant transverse displacement component (*w*).
Rotations about the x- and y-axes are represented as Φ_x and Φ_y, while the slopes in both directions are defined by variables β_x and β_y, respectively (i.e., $\Phi_x = \beta_y$ and $\Phi_y = \beta_x$).
Equation (6-a) can be rewritten in the matrix form as:

$$\begin{Bmatrix} u \\ v \\ w \end{Bmatrix} = \begin{bmatrix} z & 0 & 0 \\ 0 & z & 0 \\ 0 & 0 & 1 \end{bmatrix} \begin{Bmatrix} u_0 \\ w_0 \\ \theta_z \end{Bmatrix} \quad (7\text{-b})$$

2.2.2 Strain

The infinitesimal strain tensor can be represented as follows:

$$\begin{cases} \varepsilon_x = \frac{\partial u(x,y,z)}{\partial x} = z\frac{\partial \beta_x(x,y)}{\partial x} \\ \varepsilon_y = \frac{\partial v(x,y,z)}{\partial y} = z\frac{\partial \beta_y(x,y)}{\partial y} \\ \gamma_{xy} = \frac{\partial u(x,y,z)}{\partial y} + \frac{\partial v(x,y,z)}{\partial x} = z\left(\frac{\partial \beta_x(x,y)}{\partial y} + \frac{\partial \beta_y(x,y)}{\partial x}\right) \\ \gamma_{xz} = \beta_x(x,y) + \frac{\partial w(x,y)}{\partial x} \\ \gamma_{yz} = \beta_y(x,y) + \frac{\partial w(x,y)}{\partial y} \end{cases} \quad (7)$$

The bending curvatures are given by equations:

$$K_x = \frac{\partial \beta_x(x,y)}{\partial x}; K_y = \frac{\partial \beta_y(x,y)}{\partial y}; K_{xy} = \frac{\partial \beta_x(x,y)}{\partial y} + \frac{\partial \beta_y(x,y)}{\partial x} \quad (8)$$

2.2.3 Constitutive law

In the state of plane stress and for isotropic materials, which are commonly accepted assumptions for analysing thin structures such as beams, plates, and shells, the stress–strain relationship equations of the Reissner-Mindlin theory are given by:

$$\begin{Bmatrix} M_x \\ M_y \\ M_{xy} \\ T_x \\ T_y \end{Bmatrix} = \frac{Eh^3}{12(1-\nu^2)} \begin{bmatrix} 1 & \nu & 0 & 0 & 0 \\ \nu & 1 & 0 & 0 & 0 \\ 0 & 0 & \frac{1-\nu}{2} & 0 & 0 \\ 0 & 0 & 0 & \frac{6\kappa}{h^2}(1-\nu) & 0 \\ 0 & 0 & 0 & 0 & \frac{6\kappa}{h^2}(1-\nu) \end{bmatrix} \begin{Bmatrix} K_x \\ K_y \\ K_{xy} \\ \gamma_{xz} \\ \gamma_{yz} \end{Bmatrix} \quad (9)$$

The variables used in this equation are as follows:

- *E* and *v* represent the Young's modulus and Poisson ratio, respectively.
- *h* denotes thickness of the plate.
- *K* represents the 'shear factor', which is usually taken as *K* = 5/6, unless otherwise specified.
- M_x, M_y, M_{xy}, T_x, T_y represent the bending moments, torsional moment, and shear forces per unit length, respectively.

2.2.4 Strain and displacement fields

The first nine bi-harmonic solutions of the Airy function yield functions related to the nine parameters of the interpolation polynomials of the stress and deformation fields, ultimately allowing integration of the displacement field. The interpolation polynomials for the deformation fields related to bending (Appendix A) were obtained by introducing these functions into equation (5) and are expressed as follows:

$$\begin{Bmatrix} K_x(x,y) \\ K_y(x,y) \\ K_{xy}(x,y) \end{Bmatrix} = \frac{1}{zE}\begin{bmatrix} 0 & 0 & 0 & 1 & 0 & 0 & -6\nu x & 6y & 2x^2 - 2\nu y^2 \\ 0 & 0 & 0 & 0 & 1 & 0 & 6x & -6\nu y & -2\nu x^2 + 2y^2 \\ 0 & 0 & 0 & 0 & 0 & 2 & 0 & 0 & -8\nu xy \end{bmatrix} \begin{Bmatrix} a_1 \\ a_2 \\ a_3 \\ a_4 \\ a_5 \\ a_6 \\ a_7 \\ a_8 \\ a_9 \end{Bmatrix} \tag{10}$$

These fields consistently satisfy the equilibrium conditions in equation (1) and the kinematic condition of compatibility:

$$\frac{\partial^2 K_x}{\partial y^2} + \frac{\partial^2 K_y}{\partial x^2} = \frac{\partial^2 K_{xy}}{\partial x \partial y} \tag{11}$$

The polynomial field interpolation for the shear-related deformation field, which is detailed in Appendix B, was obtained by satisfying the remaining two kinematic compatibility equations:

$$\begin{cases} \frac{\partial^2 \gamma_{xz}}{\partial x \partial y} - \frac{\partial^2 \gamma_{yz}}{\partial x^2} + \frac{\partial K_{xy}}{\partial x} = 2\frac{\partial K_x}{\partial y} \\ \frac{\partial^2 \gamma_{yz}}{\partial x \partial y} - \frac{\partial^2 \gamma_{xz}}{\partial y^2} + \frac{\partial K_{xy}}{\partial y} = 2\frac{\partial K_y}{\partial x} \end{cases} \tag{12}$$

These can be represented in the matrix form as follows:

$$\begin{Bmatrix} \gamma_{xz}(x,y) \\ \gamma_{yz}(x,y) \end{Bmatrix} = \frac{1}{zE}\begin{bmatrix} 0 & 0 & 0 & 0 & 0 & 0 & -6y^2 & 0 & 0 \\ 0 & 0 & 0 & 0 & 0 & 0 & 0 & -6x^2 & 0 \end{bmatrix} \begin{Bmatrix} a_1 \\ a_2 \\ a_3 \\ a_4 \\ a_5 \\ a_6 \\ a_7 \\ a_8 \\ a_9 \end{Bmatrix} \tag{13}$$

By substituting the deformation fields from equations (10) and (13) into equation (7) and integrating them, the following displacement fields are obtained:

$$\{q(x,y)\} = \frac{1}{zE}[f(x,y)]\{a_i\} \tag{14-a}$$

The displacement field is:

$$\{q(x,y)\} = \begin{Bmatrix} w(x,y) \\ \beta_x(x,y) \\ \beta_y(x,y) \end{Bmatrix} \tag{14-b}$$

The nodal coordinates are as follows:

$$[F(x,y)] = \begin{bmatrix} 1 & -x & -y & \frac{-x^2}{2} & \frac{-y^2}{2} & -xy & -3xy^2+\nu x^3 & -3yx^2+\nu y^3 & \frac{-1}{6}(x^4+y^4)+\nu x^2y^2 \\ 0 & 1 & 0 & x & 0 & y & -3\nu x^2+3y^2 & 6xy & \frac{2}{3}x^3-2\nu xy^2 \\ 0 & 0 & 1 & 0 & y & x & 6xy & -3\nu y^2+3x^2 & \frac{2}{3}y^3-2\nu yx^2 \end{bmatrix} \quad (14\text{-c})$$

The nine independent constants defined as follows:

$$\{a_i\}^T = \{a_1 \quad a_2 \quad a_3 \quad a_4 \quad a_5 \quad a_6 \quad a_7 \quad a_8 \quad a_9\} \quad (14\text{-d})$$

Given the nodal coordinates corresponding to node (x_i, y_i), and applying equation (14-a), the nodal displacement vector at the element level is given as follows:

$$\{q^e\} = \frac{1}{zE}\begin{bmatrix} f(x_1,y_1) \\ f(x_2,y_2) \\ f(x_3,y_3) \end{bmatrix}\{a_i\} \quad (15\text{-a})$$

where $\{q^e\}$ is the nodal displacement vector, represented as:

$$\{q^e\}^T = \{w_1 \quad \beta_{x1} \quad \beta_{y1} \quad w_2 \quad \beta_{x2} \quad \beta_{y2} \quad w_3 \quad \beta_{x3} \quad \beta_{y3}\} \quad (15\text{-b})$$

The matrix of nodal coordinates is denoted as follows:

$$[A] = \frac{1}{zE}\begin{bmatrix} f(x_1,y_1) \\ f(x_2,y_2) \\ f(x_3,y_3) \end{bmatrix} \quad (16)$$

The values of parameter a_i can be deduced from equations (15-a) and (16), respectively:

$$\{a_i\} = [A]^{-1}\{q^e\} \quad (17)$$

The kinematic equations can be rewritten using the following transformations:

- displacement field

$$\{q(x,y)\} = \begin{Bmatrix} w(x,y) \\ \beta_x(x,y) \\ \beta_y(x,y) \end{Bmatrix} = [f(x,y)][A]^{-1}\{q^e\} \quad (18)$$

- curvature–moment fields

$$\begin{Bmatrix} k_x(x,y) \\ k_y(x,y) \\ k_{xy}(x,y) \end{Bmatrix} = [B_f][A]^{-1}\{q^e\} \quad (19\text{-a})$$

where

$$[B_f] = \frac{1}{zE}\begin{bmatrix} 0 & 0 & 0 & 1 & 0 & 0 & -6\nu x & 6y & 2x^2-2\nu y^2 \\ 0 & 0 & 0 & 0 & 1 & 0 & 6x & -6\nu y & -2\nu x^2+2y^2 \\ 0 & 0 & 0 & 0 & 0 & 2 & 0 & 0 & -8\nu xy \end{bmatrix} \quad (19\text{-b})$$

- shear strain fields

$$\begin{Bmatrix} \gamma_{xz}(x,y) \\ \gamma_{yz}(x,y) \end{Bmatrix} = [B_c][A]^{-1}\{q^e\} \quad (20\text{-a})$$

where

$$[B_c] = \frac{1}{zE}\begin{bmatrix} 0 & 0 & 0 & 0 & 0 & 0 & -6y^2 & 0 & 0 \\ 0 & 0 & 0 & 0 & 0 & 0 & 0 & -6x^2 & 0 \end{bmatrix} \quad (20\text{-b})$$

2.2.5 Elementary stiffness matrix

The elementary stiffness matrix was derived using the discretised principle of virtual internal work and can be presented as follows:

- bending stiffness

$$\left[K_f^e\right] = [A^{-1}]^T \left[\iint \left[B_f\right]^T \left[D_f\right]\left[B_f\right] dxdy\right] [A^{-1}] \quad (21)$$

- shear stiffness

$$[K_c^e] = [A^{-1}]^T [\iint [B_c]^T [D_c][B_c] dxdy][A^{-1}] \quad (22)$$

Given that $\left[D_f\right] = \frac{Eh^3}{12(1-\nu^2)}\begin{bmatrix} 1 & \nu & 0 \\ \nu & 1 & 0 \\ 0 & 0 & \frac{1-\nu}{2} \end{bmatrix}$ and $[D_c] = \frac{E\kappa h}{2(1+\nu)}\begin{bmatrix} 1 & 0 \\ 0 & 1 \end{bmatrix}$ the expressions for $\left[\iint \left[B_f\right]^T \left[D_f\right]\left[B_f\right] dxdy\right]$ and $[\iint [B_c]^T [D_c][B_c] dxdy]$ were evaluated through the analytical integration of various components resulting from the matrix products $\left[B_f\right]^T \left[D_f\right]\left[B_f\right]$ and $[B_c]^T [D_c][B_c]$. These expressions can be written as $H_{(\alpha+1)(\beta+1)} = Cx^{\alpha} y^{\beta}$, where α and β are exponents, and C is a constant.

2.3 Sandwich Panels-equivalent properties

A sandwich structure composed of two thin solid face sheets separated by a cellular core was considered (Figure 3). The equivalent modulus of elasticity and Poisson's ratio of the sandwich plate are expressed as follows:

$$\tilde{E} = \frac{(2E_s h_s)+(E_c h_c)}{h_t} \quad (23\text{-a})$$

$$\tilde{\nu} = \frac{(2\nu_s h_s)+(\nu_c h_c)}{h_t} \quad (2\text{b-b})$$

Where E_s and E_c are the moduli of elasticity, h_s and h_c are the thicknesses, and v_s and v_c are the Poisson's ratios of the skin and core of the sandwich beam, respectively.

3 Numerical results and discussion

This section is divided into two sub-sections. The first is dedicated to comparing the proposed model with the analytical solutions and other numerical approaches for sandwich plates. The second sub-section focuses on the parametric study.

3.1 Comparison with analytical and numerical solutions

3.1.1 Example 1: Simply supported sandwich plate under a centre load

In the first example, an analysis was conducted on a simply supported sandwich plate subjected to a central load to predict the maximum deflection at the mid-span of the plate.
A polyurethane foam core with a thickness of 17,5 mm sandwiched between two steel face sheets, each with a thickness of 0,5 mm, was considered. The plate had a span length of 200 mm and a width of 50 mm (Figure 3).
Table 1 presents the material characteristics of the sandwich plates along with their corresponding equivalent properties for all examples considered.

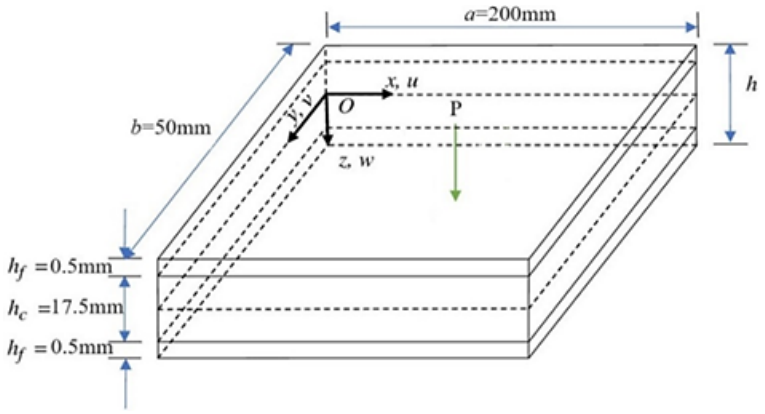

Figure 3. Simply supported sandwich plate under a centre load

Table 1. Material characteristics and corresponding equivalent properties of sandwich plates

Mechanical properties	Skin (s) (Polyurethane foam)	Core (c) (Steel)	Equivalent material properties
E (GPa)	210	160	162,7027
v	0,30	0,34	0,33

For validation, the maximum deflection of a sandwich plate subjected to a central load was evaluated and compared with solutions from the layer-wise theory and other numerical methods. The results are summarised in Table 2 and Figure 4. In the table and figure, 'TBT' refers to the outcomes of applying the Timoshenko beam theory, which included shear deformation, while 'EBT' refers to the results of applying the Euler–Bernoulli beam theory, which excludes shear deformation. 'CSB Homog.' and 'CSB Comp.' denote the maximum deflections calculated using the software cross-section beam (CSB) developed by El Fatimi and Zenzri [30], which considers both homogenised and stratified sections. As indicated in Table 2 and Figure 4, the results of the proposed method corroborate the results of both the analytical solutions and numerical approaches.
NB: Cross-section beam (CSB) solutions are based on solutions to the Saint-Venant equations, considering section deformations after loading (in contrast to other assumptions that consider that a straight section remains straight).

Table 2. Maximum deflections of simply supported sandwich plate subjected to a centre load

Deflection (mm)	Analytical solutions	FEM [31]		Present FEM	CSB Homog. [30]	CSB Comp. [30]
		TBT	EBT			
Bending deflection (skins)	0,05651	0,05984	0,05824			
Shear deflection (core)	0,00136					
Total defl. @ midspan	0,05787			0,05702	0,0601	0,0482

TBT: Timoshenko beam theory, EBT: Euler–Bernoulli beam theory, CSB Homo.: Cross-section beam, homogenous, CSB Comp.: Cross-section beam, composite.

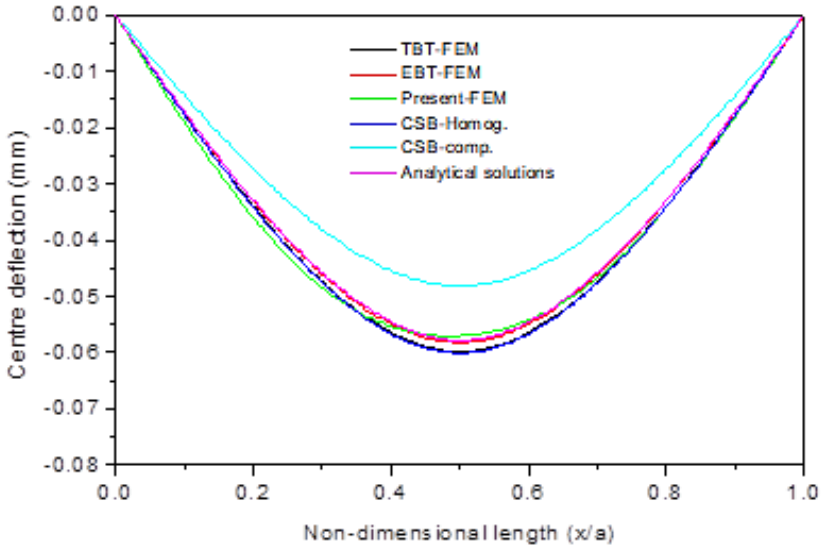

Figure 4. Maximum deflections of simply supported sandwich plate under a centre load

3.1.2 Example 2: Simply supported sandwich plate under a uniformly distributed load

In the second example, the deflection of a simply supported sandwich plate under a uniformly distributed load was investigated (Figure 5).

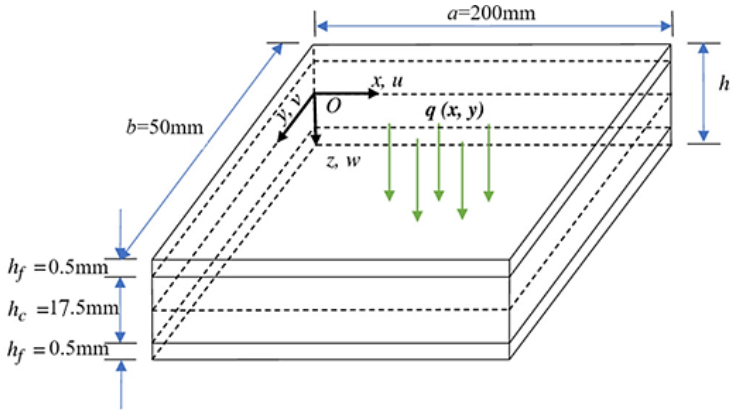

Figure 5. Simply supported sandwich plate under a uniformly distributed load

Table 3 and Figure 6 display a comparison that indicates a favourable agreement between the predicted values obtained using the proposed model and those obtained using TBT, EBT, CSB Homog., and CSB Comp., along with the analytical solutions.

Table 3. Maximum deflections of simply supported sandwich plate under a uniformly distributed load

Deflection (mm)	Analytical solutions	FEM [31]		Present FEM	CSB Homog. [30]	CSB Comp. [30]
		TBT	EBT			
Bending deflection (skins)	7,06433	7,3514	7,28030			
Shear deflection (core)	0,00068					
Total defl. @ midspan	7,06500			7,4117	7,4692	5,9950

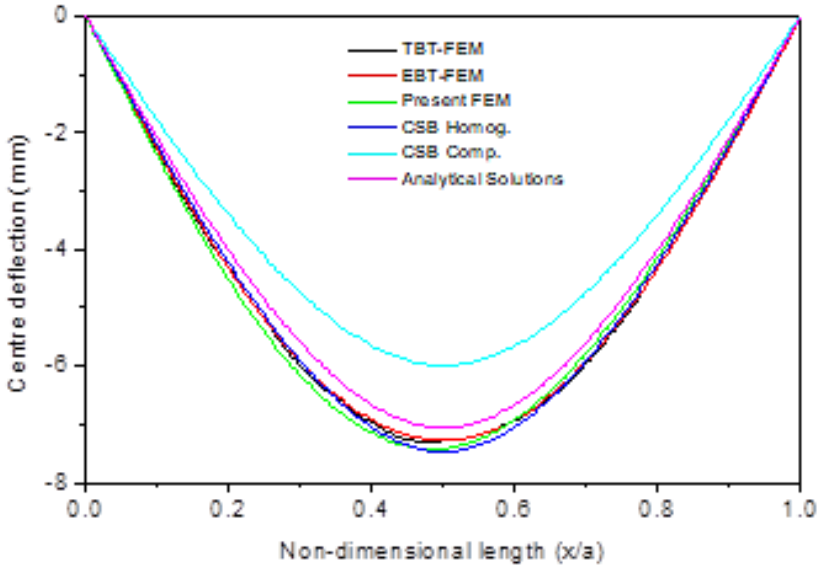

Figure 6. Maximum deflections of simply supported sandwich plate under a uniformly distributed load

3.1.3 Example 3: Clamped–clamped sandwich plate subjected to a concentrated load

In this example, a clamped–clamped (C–C) sandwich plate subjected to a concentrated load was analysed (Figure 7). A comparison of the results with reference solutions demonstrates the precision and accuracy of the proposed model (Table 4 and Figure 8).

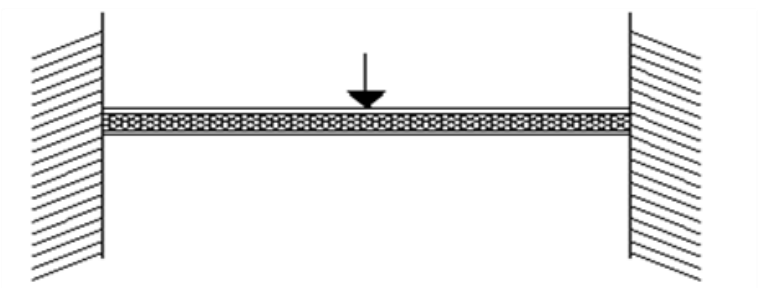

Figure 7. Clamped-clamped sandwich plate under a concentrated load

Table 4. Maximum deflections of clamped-clamped sandwich plate under a concentrated load

Deflection (mm)	Analytical solutions	FEM [31]		Present FEM	CSB Homog. [30]	CSB Comp. [30]
		TBT	EBT			
Bending deflection (skins)	0,01413	0,01616	0,01456			
Shear deflection (core)	0,00136					
Total defl. @ midspan	0,01549			0,01432	0,0164	0,0131

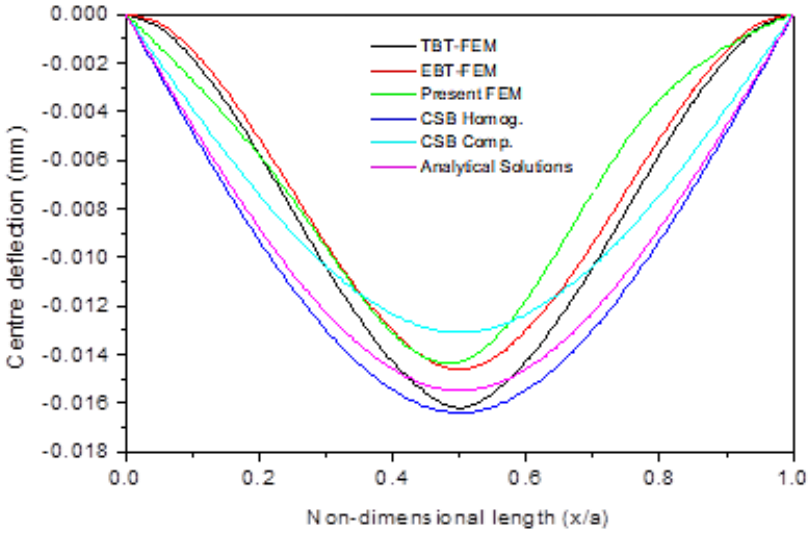

Figure 8. Maximum deflections of clamped–clamped sandwich plate under a concentrated load

3.1.4 Example 4: Clamped–clamped sandwich plate subjected to distributed uniform load

The fourth case study examined the bending behaviour of a clamped–clamped sandwich plate subjected to a distributed uniform load (Figure 9).

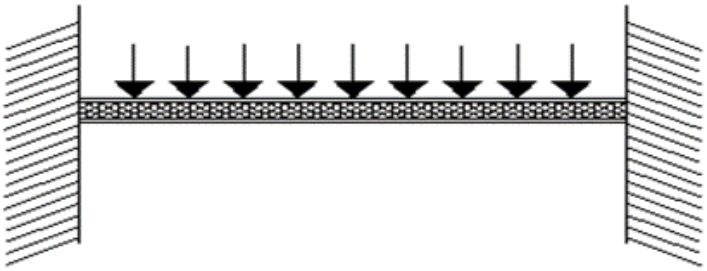

Figure 9. Clamped-clamped sandwich plate subjected to a distributed uniform load

Table 5 and Figure 10 show that the current finite element method produces favourable results compared with the reference solutions.

Table 5. Maximum deflections of clamped-clamped sandwich plate subjected to a distributed uniform load

Deflection (mm)	**Analytical solutions**	**FEM [31]**		**Present FEM**	**CSB Homog. [30]**	**CSB Comp. [30]**
		TBT	**EBT**			
Bending deflection (skins)	1,41287	1,6160	1,45610			
Shear deflection (core)	0,00068					
Total defl. @ midspan	1,41354			1,53228	1,6449	1,3121

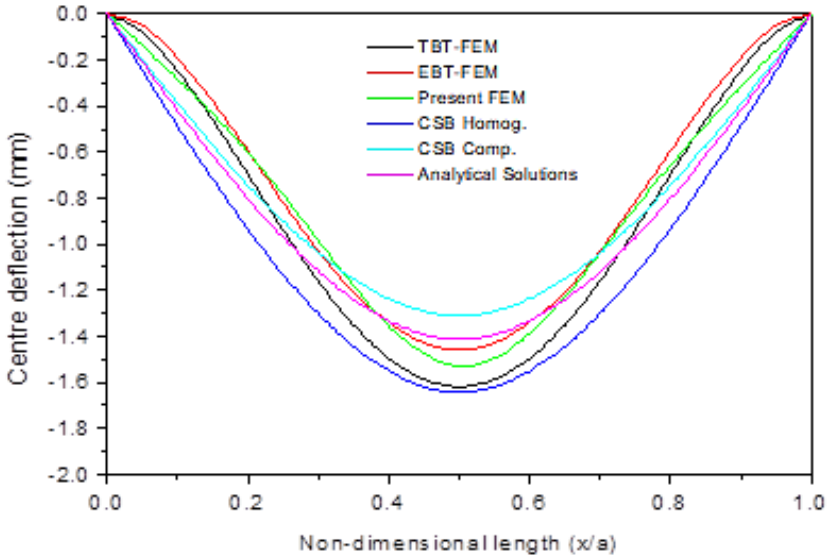

Figure 10. Maximum deflections of clamped-clamped sandwich plate subjected to a distributed uniform load

3.1.5 Example 5: Clamp-free sandwich plate with a point load applied at the free end

The last example considers a free-span sandwich panel with a point load applied at the free end (Figure 11). The comparisons in Table 6 and Figure 12 support and confirm the precision and performance of the proposed finite element model.

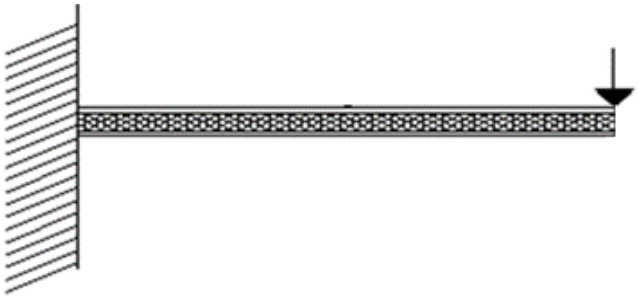

Figure 11. Clamped-free sandwich plate with a point load applied at the free end

Table 6. Maximum deflections of clamped-free sandwich plate with a point load applied at the free end

Deflection (mm)	Analytical solutions	FEM [31]		Present FEM	CSB Homog. [30]	CSB Comp. [30]
		TBT	EBT			
Bending deflection (skins)	0,90423	0,93828	0,93188			
Shear deflection (core)	0,00136					
Total defl. @ midspan	0,90559			0,91054	0,9394	0,7549

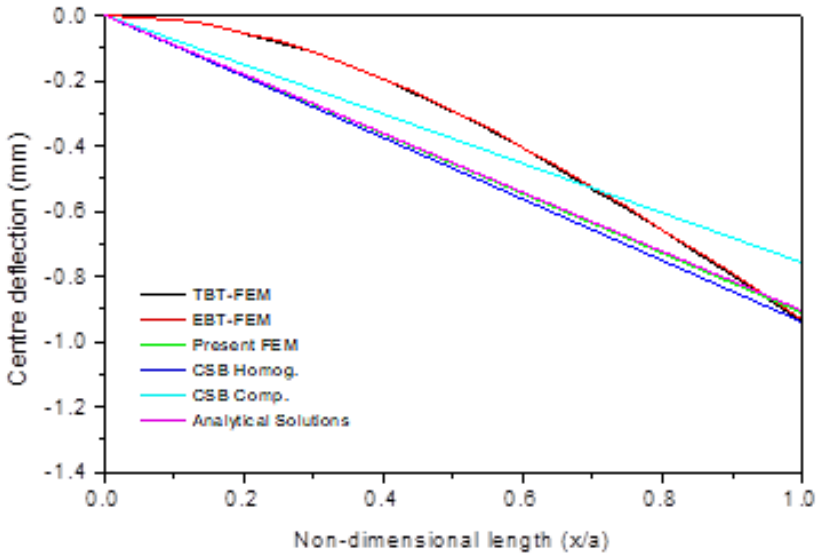

Figure 12. Maximum deflections of clamped-free sandwich plate with a point load applied at the free end

3.2 Parametric study

Following the validation of the finite element model using extant analytical solutions and numerical data, the static response of the sandwich plate was examined under different boundary conditions, load types, and geometric variations, including thickness configurations, length-to-thickness ratios, and equivalent material properties. The material properties of the sandwich plate used in this section were consistent with those in the first subsection. In the (1-8-1) configuration, the core is eight times thicker than each face sheet. In the (1-3-1) configuration, the core thickness was three times that of the individual outer layers. In the (1-1-1) configuration, the sandwich structure consisted of three layers of uniform thickness.
Table 7 lists the maximum deflections of the sandwich panels under different geometric effects and boundary conditions when subjected to concentrated loads. As evident in the table, for configurations with a fixed thickness, the deflection values increase as the length-to-thickness ratio increases. Additionally, across all thickness configurations, the deflections in the (C–F) sandwich plate were greater than those observed under the other boundary conditions (S–S) and (C–C). Consequently, the plates with (C–C) boundary constraints were more sensitive to the slenderness ratio than the other boundary conditions. Furthermore, for a constant length-to-thickness ratio, increasing the core thickness reduced the deflections under all the boundary conditions examined.

Table 7. Maximum deflections of sandwich panels under different geometric effects and boundary conditions subjected to a concentrated load

Thickness configurations	L/h	Maximum deflection		
		S-S	C-C	C-F
1-8-1	10	$4{,}55 \times 10^{-2}$	$1{,}24 \times 10^{-2}$	$7{,}11 \times 10^{-1}$
	20	$3{,}56 \times 10^{-1}$	$9{,}11 \times 10^{-2}$	$5{,}66 \times 10^{0}$
	30	$1{,}19 \times 10^{0}$	$3{,}01 \times 10^{-1}$	$1{,}90 \times 10^{-1}$
	40	$2{,}83 \times 10^{0}$	$7{,}11 \times 10^{-1}$	$4{,}51 \times 10^{-1}$
	50	$5{,}52 \times 10^{0}$	$1{,}39 \times 10^{0}$	$8{,}82 \times 10^{-1}$
1-3-1	10	$4{,}30 \times 10^{-2}$	$1{,}17 \times 10^{-2}$	$6{,}71 \times 10^{-1}$
	20	$3{,}36 \times 10^{-1}$	$8{,}61 \times 10^{-2}$	$5{,}35 \times 10^{0}$
	30	$1{,}12 \times 10^{0}$	$2{,}84 \times 10^{-1}$	$1{,}79 \times 10^{1}$
	40	$2{,}67 \times 10^{0}$	$6{,}71 \times 10^{-1}$	$4{,}26 \times 10^{1}$
	50	$5{,}21 \times 10^{0}$	$1{,}31 \times 10^{0}$	$8{,}33 \times 10^{1}$

1-1-1	10	$4{,}00 \times 10^{-2}$	$1{,}09 \times 10^{-2}$	$6{,}25 \times 10^{-1}$
	20	$3{,}13 \times 10^{-1}$	$8{,}01 \times 10^{-2}$	$4{,}98 \times 10^{0}$
	30	$1{,}05 \times 10^{0}$	$2{,}64 \times 10^{-1}$	$1{,}67 \times 10^{1}$
	40	$2{,}48 \times 10^{0}$	$6{,}25 \times 10^{-1}$	$3{,}97 \times 10^{1}$
	50	$4{,}85 \times 10^{0}$	$1{,}22 \times 10^{0}$	$7{,}76 \times 10^{1}$

Figures 13-15 illustrate the effects of the length-to-thickness ratio and thickness configuration on the deflections of the (S–S), (C–C), and (C–F) sandwich plates, respectively. As observed in the figures, the deflections increase as the length-to-thickness ratio increases. The results also indicate that the maximum deflection occurred at L/h = 50. Notably, the 1-8-1 sandwich plate exhibited higher maximum deflections than the other configurations.

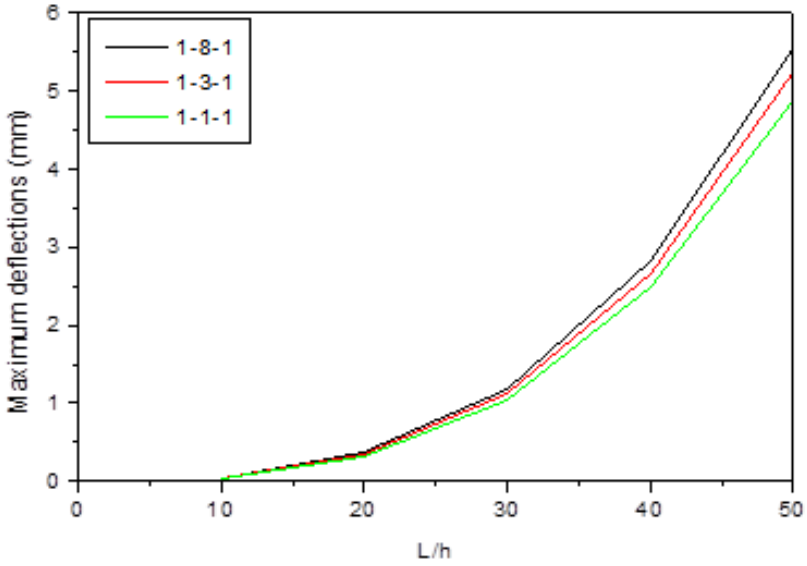

Figure 13. Variation of maximum deflections of simply supported sandwich plate under a concentrated load versus length-to-thickness ratio (L/h) and different thickness configurations

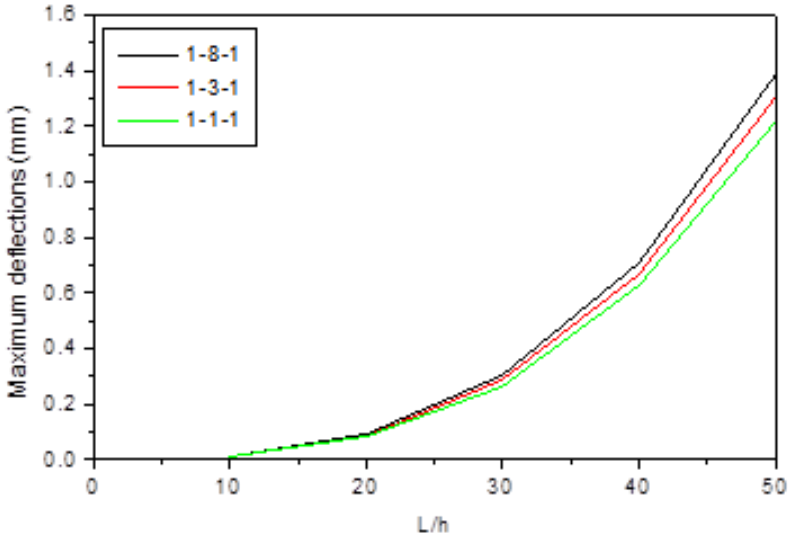

Figure 14. Variation of maximum deflections of clamped–clamped sandwich plate under a concentrated load versus length-to-thickness ratio (L/h) and different thickness configurations

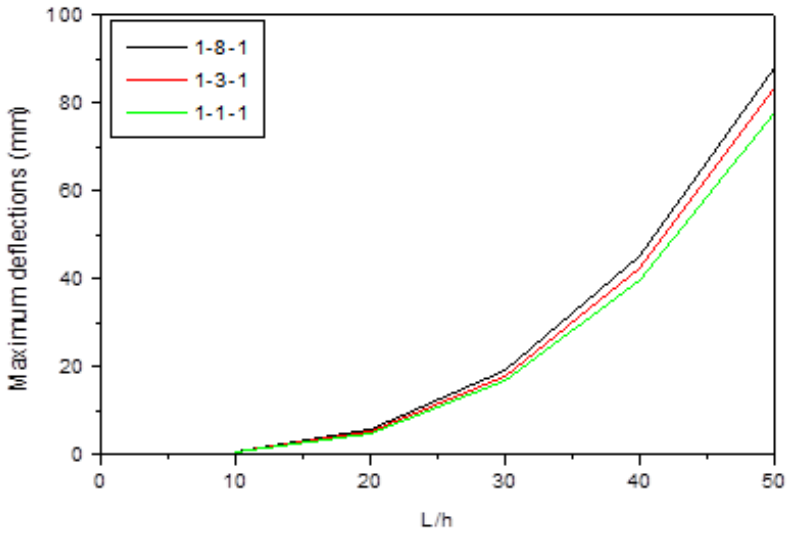

Figure 15. Variation of maximum deflection ns of clamped–free sandwich plate under a concentrated load versus length-to-thickness ratio (L/h) and different thickness configurations

Table 8 lists the maximum deflections observed for a sandwich plate under a uniformly distributed load, considering different geometric effects and boundary conditions. As the length-to-thickness ratio increased, the deflections increased across all the thickness configurations and boundary conditions. For a constant length-to-thickness ratio, increasing the core thickness resulted in lower deflections for all boundary conditions examined. Similar results are illustrated in Figures 16-18.

Table 8. Maximum deflections of sandwich panels under different geometric effects and boundary conditions subjected to uniformly distributed load

Thickness configurations	L/h	Maximum deflections		
		S-S	C-C	C-F
1-8-1	10	$6{,}35 \times 10^{-3}$	$6{,}22 \times 10^{-4}$	$1{,}26 \times 10^{-2}$
	20	$9{,}60 \times 10^{-2}$	$1{,}82 \times 10^{-2}$	$8{,}22 \times 10^{-1}$
	30	$6{,}80 \times 10^{-1}$	$1{,}35 \times 10^{-1}$	$6{,}37 \times 10^{0}$
	40	$2{,}84 \times 10^{0}$	$5{,}69 \times 10^{-1}$	$2{,}70 \times 10^{+1}$
	50	$8{,}64 \times 10^{0}$	$1{,}73 \times 10^{0}$	$8{,}27 \times 10^{+1}$
1-3-1	10	$6{,}00 \times 10^{-3}$	$5{,}87 \times 10^{-4}$	$1{,}19 \times 10^{-2}$
	20	$9{,}06 \times 10^{-2}$	$1{,}72 \times 10^{-2}$	$7{,}76 \times 10^{+1}$
	30	$6{,}42 \times 10^{-1}$	$1{,}28 \times 10^{-1}$	$6{,}02 \times 10^{0}$
	40	$2{,}68 \times 10^{0}$	$5{,}37 \times 10^{-1}$	$2{,}55 \times 10^{+1}$
	50	$8{,}16 \times 10^{0}$	$1{,}64 \times 10^{0}$	$7{,}81 \times 10^{+1}$
1-1-1	10	$5{,}58 \times 10^{-3}$	$5{,}46 \times 10^{-4}$	$1{,}11 \times 10^{-2}$
	20	$8{,}44 \times 10^{-2}$	$1{,}60 \times 10^{-2}$	$7{,}23 \times 10^{-1}$
	30	$5{,}97 \times 10^{-1}$	$1{,}19 \times 10^{-1}$	$5{,}60 \times 10^{0}$
	40	$2{,}50 \times 10^{0}$	$5{,}00 \times 10^{-1}$	$2{,}38 \times 10^{+1}$
	50	$7{,}60 \times 10^{0}$	$1{,}52 \times 10^{0}$	$7{,}27 \times 10^{+1}$

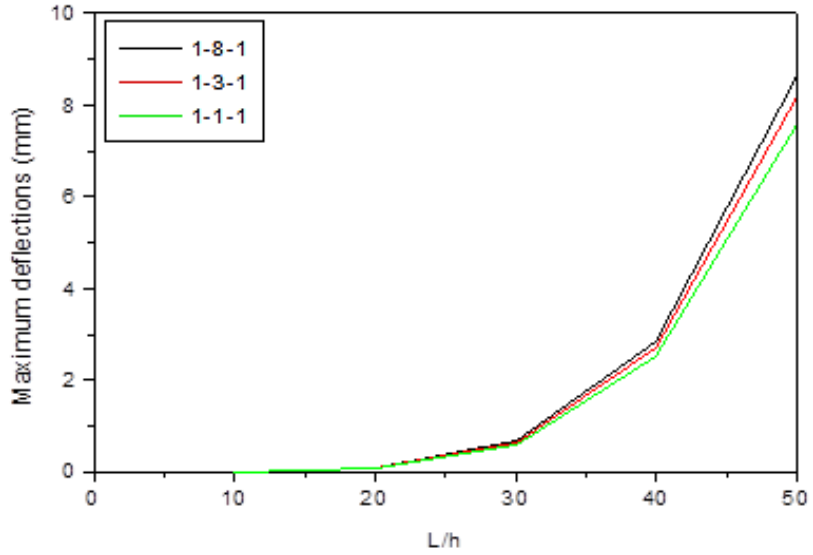

Figure 16. Variation of maximum deflections of simply supported sandwich plate under uniformly distributed load versus length-to-thickness ratio (L/h) and different thickness configurations

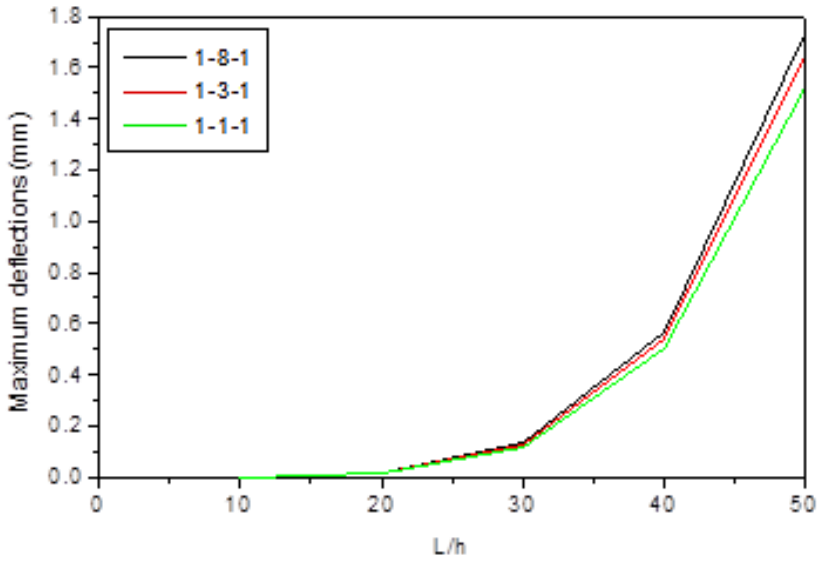

Figure 17. Variation of maximum deflections of clamped–clamped sandwich plate under uniformly distributed load versus length-to-thickness ratio (L/h) and different thickness configurations

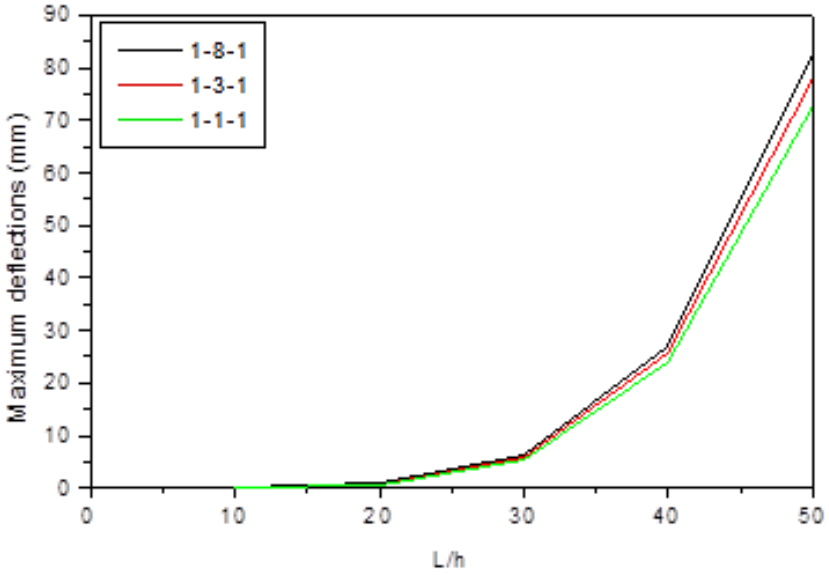

Figure 18. Variation of maximum deflections of clamped–free sandwich plate under uniformly distributed load versus length-to-thickness ratio (L/h) and different thickness configurations

Table 9 and Figures 19-21 illustrate the impact of the overall thickness of the sandwich plate and the effect of thickness configuration on the maximum deflections under different boundary conditions under a concentrated load. Increasing the total thickness decreased the deflections, because a thicker sandwich plate is less flexible. For a constant total thickness, increasing the core thickness decreased the deflections across all boundary conditions.
Additionally, the maximum deflections for the sandwich plate (C-F) are greater than those for the other boundary conditions (S-S and C-C). This is because variations in the boundary conditions affect the rigidity of the plate, which, in turn, influences its deflection.

Table 9. Variation of maximum deflections of sandwich panels with total thickness under different boundary conditions and a concentrated load

Thickness configuration	h_t	Maximum deflections		
		S-S	C-C	C-F
1-8-1	0,01	$3{,}53 \times 10^{8}$	$8{,}82 \times 10^{7}$	$5{,}64 \times 10^{9}$
	0,02	$4{,}42 \times 10^{7}$	$1{,}10 \times 10^{7}$	$7{,}07 \times 10^{8}$
	0,03	$1{,}30 \times 10^{7}$	$3{,}25 \times 10^{6}$	$2{,}08 \times 10^{8}$
	0,04	$5{,}51 \times 10^{6}$	$1{,}38 \times 10^{6}$	$8{,}81 \times 10^{7}$
	0,05	$2{,}82 \times 10^{6}$	$7{,}06 \times 10^{5}$	$4{,}52 \times 10^{7}$
1-3-1	0,01	$3{,}33 \times 10^{8}$	$8{,}33 \times 10^{7}$	$5{,}33 \times 10^{9}$
	0,02	$4{,}17 \times 10^{7}$	$1{,}04 \times 10^{7}$	$6{,}67 \times 10^{8}$
	0,03	$1{,}23 \times 10^{7}$	$3{,}07 \times 10^{6}$	$1{,}97 \times 10^{8}$
	0,04	$5{,}20 \times 10^{6}$	$1{,}30 \times 10^{6}$	$8{,}32 \times 10^{7}$
	0,05	$2{,}67 \times 10^{6}$	$6{,}66 \times 10^{5}$	$4{,}27 \times 10^{7}$
1-1-1	0,01	$3{,}10 \times 10^{8}$	$7{,}75 \times 10^{7}$	$4{,}96 \times 10^{9}$
	0,02	$3{,}88 \times 10^{7}$	$9{,}71 \times 10^{6}$	$6{,}21 \times 10^{8}$
	0,03	$1{,}14 \times 10^{7}$	$2{,}86 \times 10^{6}$	$1{,}83 \times 10^{8}$
	0,04	$4{,}84 \times 10^{6}$	$1{,}21 \times 10^{6}$	$7{,}75 \times 10^{7}$
	0,05	$2{,}48 \times 10^{6}$	$6{,}20 \times 10^{5}$	$3{,}97 \times 10^{7}$

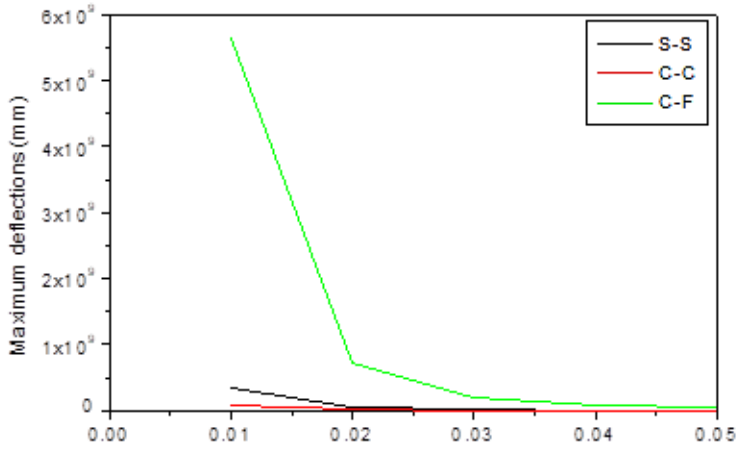

Figure 19. Effect of total thickness (h_t) on maximum deflection of sandwich panels under concentrated loads and various boundary conditions (1-8-1)

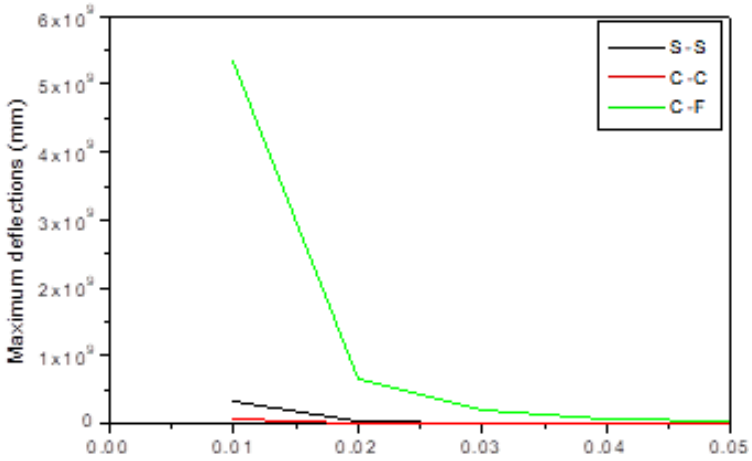

Figure 20. Effect of total thickness (h_t) on maximum deflection of sandwich panels under concentrated loads and different boundary conditions (1-3-1)

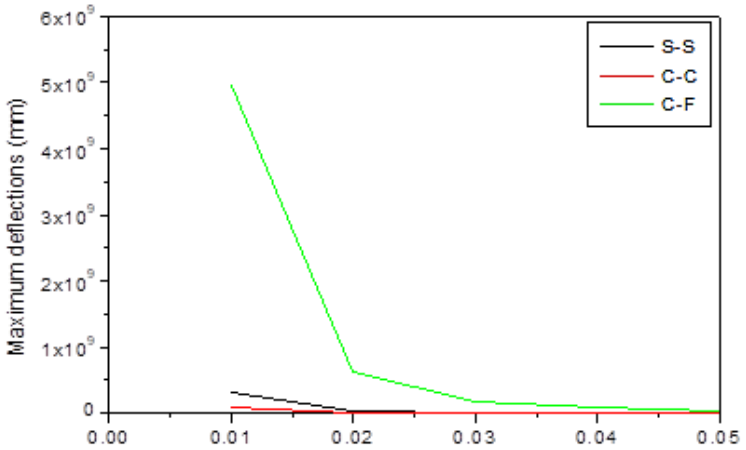

Figure 21. Effect of total thickness (h_t) on maximum deflection of sandwich panels under concentrated loads and various boundary conditions (1-1-1)

Table 10 demonstrates the significant impact of varying the total thickness, particularly the core thickness, on the maximum deflection of the sandwich plate. Specifically, increasing these thicknesses (denoted as 'h_t' and 'h_c', respectively) decreased the deflection. This highlights the considerable effect of the thickness parameters, which enhance the sandwich plate's rigidity and reduce deflection. In addition, deflections correlate with changes in boundary conditions, as altering them affects the plate's rigidity and, consequently, its flexibility.

Table 10. Variation of maximum deflections of sandwich panels with total thickness under different boundary conditions and uniformly distributed load

Thickness configuration	h_t	Maximum deflections		
		S-S	C-C	C-F
1-8-1	0,01	$4{,}41 \times 10^{10}$	$8{,}82 \times 10^{9}$	$4{,}23 \times 10^{11}$
	0,02	$5{,}52 \times 10^{9}$	$1{,}10 \times 10^{9}$	$5{,}30 \times 10^{10}$
	0,03	$1{,}63 \times 10^{9}$	$3{,}25 \times 10^{8}$	$1{,}56 \times 10^{10}$
	0,04	$6{,}88 \times 10^{8}$	$1{,}38 \times 10^{8}$	$6{,}61 \times 10^{9}$
	0,05	$3{,}53 \times 10^{8}$	$7{,}06 \times 10^{7}$	$3{,}39 \times 10^{9}$
1-3-1	0,01	$4{,}16 \times 10^{10}$	$8{,}33 \times 10^{9}$	$4{,}00 \times 10^{11}$
	0,02	$5{,}21 \times 10^{9}$	$1{,}04 \times 10^{9}$	$5{,}01 \times 10^{10}$
	0,03	$1{,}54 \times 10^{9}$	$3{,}07 \times 10^{8}$	$1{,}47 \times 10^{10}$
	0,04	$6{,}50 \times 10^{8}$	$1{,}30 \times 10^{8}$	$6{,}24 \times 10^{9}$
	0,05	$3{,}33 \times 10^{8}$	$6{,}66 \times 10^{7}$	$3{,}20 \times 10^{9}$
1-1-1	0,01	$3{,}88 \times 10^{10}$	$7{,}75 \times 10^{9}$	$3{,}72 \times 10^{11}$
	0,02	$4{,}85 \times 10^{9}$	$9{,}71 \times 10^{8}$	$4{,}66 \times 10^{10}$
	0,03	$1{,}43 \times 10^{9}$	$2{,}86 \times 10^{8}$	$1{,}37 \times 10^{10}$
	0,04	$6{,}05 \times 10^{8}$	$1{,}21 \times 10^{8}$	$5{,}81 \times 10^{9}$
	0,05	$3{,}10 \times 10^{8}$	$6{,}20 \times 10^{7}$	$2{,}98 \times 10^{9}$

Figures 22-24 illustrate the impact of varying the total thickness on the deflection of the sandwich plate under different boundary conditions for (1-8-1), (1-3-1), and (1-1-1) thickness configurations, respectively. As noted previously, for a constant boundary condition, increasing the plate thickness increased the deflection. In addition, the deflections observed in the C-F configuration were greater than those observed with the other boundary conditions.

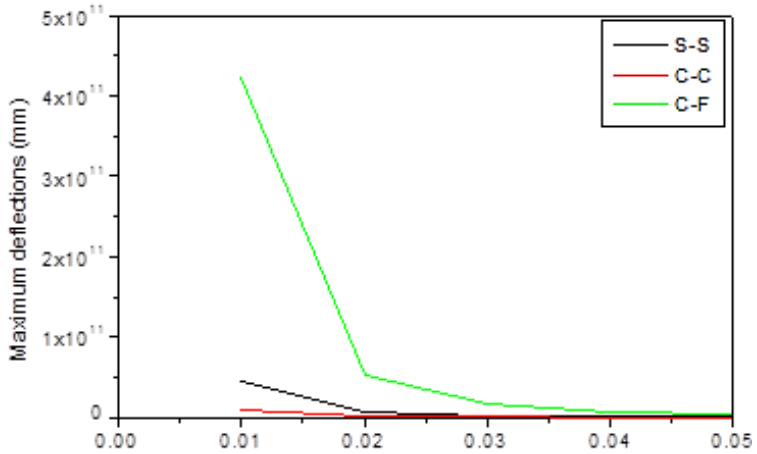

Figure 22. Effect of total thickness (h_t) on maximum deflections of sandwich panels under uniform distributed load and various boundary conditions (1-8-1)

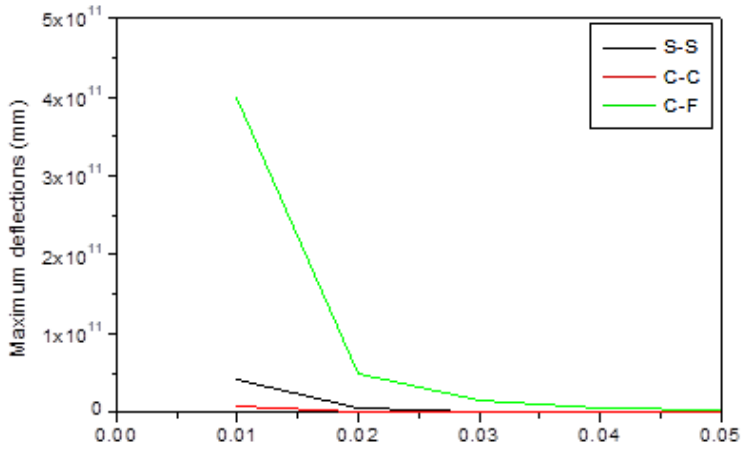

Figure 23. Effect of total thickness (h_t) on maximum deflections of sandwich panels under uniform distributed load and various boundary conditions (1-3-1)

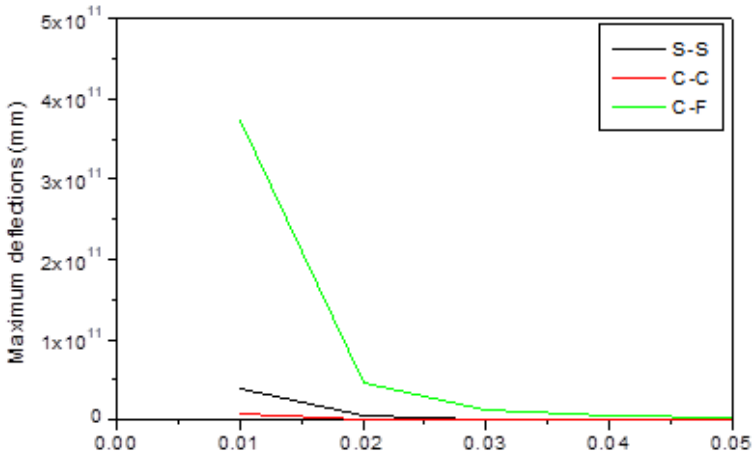

Figure 24. Effect of total thickness (h_t) on maximum deflections of sandwich panels under uniform distributed load and various boundary conditions (1-1-1)

4 Conclusion

This study conducted a comprehensive investigation of the static behaviour of sandwich plates by developing a new triangular finite element model. This study presents novel numerical solutions and explicit formulas that have not been previously reported. The study also examined the effects of geometrical parameters such as thickness configurations, length-to-thickness ratio, end boundaries, and load conditions, on the static behaviour of sandwich plates.
The following conclusions are drawn:

- For a constant-thickness configuration, the deflection increased with an increase in the length-to-thickness ratio. The maximum deflection values were obtained at (L/h = 50)
- For a constant length-to-thickness ratio, increasing the core thickness led to a decrease in the deflections under all examined boundary conditions (S-S, C-C, and C-F).
- The deflections increased as the total thickness decreased. The minimum deflection values occurred at h_t = 0,05 for all examined boundary conditions. The maximum deflection values were obtained at h = 0,01 mm.
- A simultaneous increase in the total thickness and core thickness of the sandwich plate corresponds to a decrease in deflections. This emphasises the substantial influence of

the thickness parameters, which reduce the flexibility of the sandwich plate and consequently the deflection levels.

- Under the constant-boundary condition, as the plate thickness increased, the deflection decreased.
- Moreover, the boundary conditions had a noticeable impact on the flexibility and deflection of the sandwich plates. Specifically, the (C-C) end condition exhibited lower deflections than the other boundary conditions; whereas, the (C-F) end condition resulted in a more flexible sandwich plate with higher deflection values. Hence, the stiffness characteristics of the system play a pivotal role in determining the deflections of the sandwich plates.

In the design of sandwich plates, appropriate selection of the thickness configuration, core thickness, loading and boundary conditions, and aspect ratio enables the tailoring of geometrical characteristics to minimise deflections in this type of structure.
Overall, this study provides valuable insights into the static behaviour of sandwich plates and offers guidance for optimising their design and performance for various applications.

Appendix A

Equilibrium equations for constraints derived from the Airy function: $\varphi(x,y)=P_{kl}(x,y)$

a_k	$\varphi(x,y)=$	Constraints			Deformations		
k	$P_{xl}(x,y)$	$\sigma_x=\frac{\partial^2\varphi}{\partial y^2}$	$\sigma_y=\frac{\partial^2\varphi}{\partial x^2}$	$\tau_{xy}=\frac{\partial^2\varphi}{\partial x\partial y}$	$\varepsilon_x=\frac{1}{E}\left(\frac{\partial^2\varphi}{\partial y^2}-\nu\frac{\partial^2\varphi}{\partial x^2}\right)$	$\varepsilon_y=\frac{1}{E}\left(\frac{\partial^2\varphi}{\partial x^2}-\nu\frac{\partial^2\varphi}{\partial y^2}\right)$	$\gamma_{xy}=\frac{2(1+\nu)}{E}-\frac{\partial^2\varphi}{\partial x\partial y}$
1	1	0	0	0	0	0	0
2	x	0	0	0	0	0	0
3	y	0	0	0	0	0	0
4	$\frac{y^2+\nu x^2}{2(1-\nu^2)}$	$\frac{1}{(1-\nu^2)}$	$\frac{\nu}{(1-\nu^2)}$	0	$\frac{1}{E}$	0	0
5	$\frac{x^2+\nu y^2}{2(1-\nu^2)}$	$\frac{\nu}{(1-\nu^2)}$	$\frac{1}{(1-\nu^2)}$	0	0	$\frac{1}{E}$	0
6	$\frac{-xy}{(1+\nu)}$	0	0	$\frac{1}{(1+\nu)}$	0	0	$\frac{2}{E}$
7	x^3	0	$6x$	0	$\frac{-6\nu x}{E}$	$\frac{6x}{E}$	0
8	y^3	$6y$	0	0	$\frac{6y}{E}$	$\frac{-6\nu y}{E}$	0
9	x^2y^2	$2x^2$	$2y^2$	$-4xy$	$\frac{2x^2-2\nu y^2}{E}$	$\frac{2y^2-2\nu x^2}{E}$	$\frac{-8\nu xy}{E}$

Appendix B

Determination of deformation fields γ_{xz} and γ_{yz}

Parameters	Kinematic compatibility		$\frac{\partial^2\gamma_{yz}}{\partial x\partial y}-\frac{\partial^2\gamma_{xz}}{\partial y^2}+\frac{\partial K_{xy}}{\partial y}=2\frac{\partial K_y}{\partial x}$		$\frac{\partial^2\gamma_{xz}}{\partial x\partial y}-\frac{\partial^2\gamma_{yz}}{\partial x^2}+\frac{\partial K_{xy}}{\partial x}=2\frac{\partial K_x}{\partial y}$	
	Deformations		$2\frac{\partial K_y}{\partial x}-\frac{\partial K_{xy}}{\partial y}$	$\frac{\partial^2\gamma_{yz}}{\partial x\partial y}-\frac{\partial^2\gamma_{xz}}{\partial y^2}$	$2\frac{\partial K_x}{\partial y}-\frac{\partial K_{xy}}{\partial x}$	$\frac{\partial^2\gamma_{xz}}{\partial x\partial y}-\frac{\partial^2\gamma_{yz}}{\partial x^2}$
	γ_{xz}	γ_{yz}				
a_1	0	0	0	0	0	0
a_2	0	0	0	0	0	0
a_3	0	0	0	0	0	0
a_4	0	0	0	0	0	0
a_5	0	0	0	0	0	0
a_6	0	0	0	0	0	0
a_7	$\frac{-6y^2}{E}$	0	$\frac{12}{E}$	$\frac{12}{E}$	0	0
a_8	0	$\frac{-6x^2}{E}$	0	0	0	0
a_9	0	0	0	0	0	0

References

[1] Linke, M.; Wohlers, W.; Reimerdes, H.-G. Finite Element for the Static and Stability Analysis of Sandwich Plates. *Journal of Sandwich Structures & Materials*, 2007, 9 (2), pp. 123-142. https://doi.org/10.1177/1099636207068419

[2] Starovoitov, E. I.; Leonenko, D. V. Deformation of an Elastoplastic Three-Layer Circular Plate in a Temperature Field. *Mechanics of Composite Materials*, 2019, 55 (4), pp. 503-512. https://doi.org/10.1007/s11029-019-09829-6

[3] Ryazantseva, M. Y.; Starovoitov, E. I. Static and Dynamic Models of Bending for Elastic Sandwich Plates. In: *Proceedings of the Second International Conference on Theoretical, Applied and Experimental Mechanics*, Gdoutos, E. (ed.). June 24-27, 2019, Mykonos, Greece, Springer, Cham.; 2019, pp. 531-542. https://doi.org/10.1007/978-3-030-21894-2_54

[4] Starovoitov, E. I.; Leonenko, D. V.; Tarlakovskii, D. V. Thermoelastic Deformation of a Circular Sandwich Plate by Local Loads. *Mechanics of Composite Materials*, 2018, 54 (3), pp. 299-312. https://doi.org/10.1007/s11029-018-9740-x

[5] Starovoitov, E. I.; Leonenko, D. V. Vibrations of Circular Composite Plates on an Elastic Foundation Under the Action of Local Loads. *Mechanics of Composite Materials*, 2016, 52 (5), pp. 665-672. https://doi.org/10.1007/s11029-016-9615-y

[6] Pham, V. V.; Belarbi, M.-O.; Avcar, M.; Civalek, Ö. An improved first-order mixed plate element for static bending and free vibration analysis of functionally graded sandwich plates. *Archive of Applied Mechanics*, 2023, 93 (6), pp. 1841-1862. https://doi.org/10.1007/s00419-022-02359-z

[7] Hadji, L.; Tounsi A. Static deflections and stress distribution of functionally graded sandwich plates with porosity. *Smart Structures and Systems*, 2021, 28 (3), pp. 343-354. https://doi.org/10.12989/SSS.2021.28.3.343

[8] Demirhan, P. A.; Taskin V., Static analysis of simply supported functionally graded sandwich plates by using four variable plate theory. *Teknik Dergi*, 2018, 30 (2), pp. 8987-9007. https://doi.org/10.18400/tekderg.396672

[9] Hirane, H. et al. On the layerwise finite element formulation for static and free vibration analysis of functionally graded sandwich plates. *Engineering with Computers*, 2022, 38 (5), pp. 3871-3899. https://doi.org/10.1007/s00366-020-01250-1

[10] Sahoo, R.; Singh, B. N. A new inverse hyperbolic zigzag theory for the static analysis of laminated composite and sandwich plates. *Composite Structures*, 2013, 105 (1), pp. 385-397. https://doi.org/10.1016/j.compstruct.2013.05.043

[11] Moradi-Dastjerdi, R.; Aghadavoudi F. Static analysis of functionally graded nanocomposite sandwich plates reinforced by defected CNT. *Composite Structures*, 2018, 200 (1), pp. 839-848. https://doi.org/10.1016/j.compstruct.2018.05.122

[12] Sahoo, R.; Singh, B. N. A new trigonometric zigzag theory for static analysis of laminated composite and sandwich plates. *Aerospace Science and Technology*, 2014, 35, pp. 15-28. https://doi.org/10.1016/j.ast.2014.03.001

[13] Nawariya, M. et al. Static and harmonic analysis of moderately thick square sandwich plate using FEM. *Advances in Materials Research*, 2023, 12 (2), pp. 83-100. https://doi.org/10.12989/amr.2023.12.2.083

[14] Gholamzadeh babaki, M. H.; Shakouri M. Free and forced vibration of sandwich plates with electrorheological core and functionally graded face layers. *Mechanics Based Design of Structures and Machines*, 2021, 49 (5), pp. 689-706. https://doi.org/10.1080/15397734.2019.1698436

[15] Kumar, R.; Lal, A.; Sutaria, B. M. Static and dynamic response analysis of corrugated core sandwich plates under patch loading. *Mechanics Based Design of Structures and Machines*, 2022, 51 (12), pp. 6729-6747. https://doi.org/10.1080/15397734.2022.2061510

[16] Temel, B.; Noori, A. R. Transient analysis of laminated composite parabolic arches of uniform thickness. *Mechanics Based Design of Structures and Machines*, 2019, 47 (5), pp. 546-554. https://doi.org/10.1080/15397734.2019.1572518

[17] Won, S. G. et al. Three-layered damped beam element for forced vibration analysis of symmetric sandwich structures with a viscoelastic core. *Finite Elements in Analysis and Design*, 2013, 68, pp. 39-51. https://doi.org/10.1016/j.finel.2013.01.004

[18] Guendouz, I.; Vidal, P.; Khebizi, M.; Guenfoud, M. Advanced Numerical Free Vibration Analysis of FG Thin-Walled I-Beams Using Refined Beam Models. *Journal of Composites Science*, 2025, 9 (1), 19. https://doi.org/10.3390/jcs9010019

[19] Guendouz, I. et al. Buckling analysis of thin-walled laminated composite or functionally graded sandwich I-beams using a refined beam theory. *Mechanics Based Design of Structures and Machines*, 2025, 53 (1), pp. 180-200. https://doi.org/10.1080/15397734.2024.2363497

[20] Boumezbeur, K.; Khebizi, M.; Guenfoud, M.; Guendouz, I. Mechanical Response of Thin Composite Beams Made of Functionally Graded Material Using Finite Element Method. *Periodica Polytechnica Civil Engineering*, 2023, 67 (4), pp. 970-982. https://doi.org/10.3311/PPci.21909

[21] Guendouz, I. et al. Analysis of torsional-bending FGM beam by 3D Saint-Venant refined beam theory. *Structural Engineering and Mechanics*, 2022, 84 (3), pp. 423-435. https://doi.org/10.12989/sem.2022.84.3.423

[22] Boumezbeur, K.; Khebizi, M.; Guenfoud, M. Finite element modeling of static and cyclic response of functionality graded material beams. *Asian Journal of Civil Engineering*, 2023, 24, pp. 579-591. https://doi.org/10.1007/s42107-022-00519-8

[23] Guendouz, I.; Khebizi, M.; Guenfoud, H.; Guenfoud, M. Analysis of FGM Cantilever Beams under Bending-torsional Behavior Using a Refined 1D Beam Theory. *Periodica Polytechnica Civil Engineering*, 2022, 66 (4), pp. 1262-1277. https://doi.org/10.3311/PPci.20595

[24] Khebizi, M.; Guenfoud, H.; Guenfoud, M.; El Fatmi, R. Three-dimensional modelling of functionally graded beams using Saint-Venant's beam theory. *Structural Engineering and Mechanics*, 2019, 72 (2), pp. 257-273. https://doi.org/10.12989/sem.2019.72.2.257

[25] Ziou, H.; Guenfoud, M. Modal behaviour of longitudinally perforated nanobeams. *Advances in Civil and Architectural Engineering*, 2023, 14 (27), pp. 143-159. https://doi.org/10.13167/2023.27.10

[26] Ziou, H.; Guenfoud, M. A complete disquisition of various parameters on the bending analysis of functionally graded nanobeams. *Academic Journal of Manufacturing Engineering*, 2023, 21 (1), pp. 19-27.

[27] Ziou, H.; Guenfoud, H. Buckling Analysis Behavior of Functionally Graded Beams. *Jordan Journal of Civil Engineering*, 2020, 14 (3), pp. 347-358.

[28] Ziou, H.; Himeur M.; Guenfoud H.; Guenfoud, M. An Efficient Finite Element Formulation Based on Deformation Approach for Bending of Functionally Graded Beams. *Journal of Solid Mechanics*, 2020, 12 (2), pp. 343-357. https://doi.org/10.22034/jsm.2019.1867884.1437

[29] Teodorescu, P. *Grands éléments finis 'GEF' pour l'élasticité plane*. [doctoral thesis], Ecole Polytechnique Fédérale de Lausanne, Department of Civil Engineering, Lausanne, Switzerland, 1982.

[30] El Fatmi; R.; Zenzri, H. On the structural behavior and the Saint Venant solution in the exact beam theory: Application to laminated composite beams. *Computers and Structures*, 2002, 80 (16-17), pp. 1441-1456. https://doi.org/10.1016/S0045-7949(02)00090-1

[31] Ziou, H.; Guenfoud, M. Simple incremental approach for analysing optimal non-prismatic functionally graded beams. *Advances in Civil and Architectural Engineering*, 2023, 14 (26), pp. 118-137. https://doi.org/10.13167/2023.26.8